Double-differential cross sections for ionization of H_2O by fast bare O ions: Comparison with continuum-distorted-wave eikonal-initial-state calculations in prior and post forms

S. Nandi,[1] S. Biswas,[1] A. Khan,[1] J. M. Monti,[2] C. A. Tachino,[2] R. D. Rivarola,[2] D. Misra,[1] and L. C. Tribedi[1,*]

[1]*Tata Institute of Fundamental Research, Homi Bhabha Road, Colaba, Mumbai 400 005, India*

[2]*Institute de Fisica Rosario (CONICET-UNR), Universidad Nacional de Rosario, 2000 Rosario, Argentina*

(Received 27 March 2013; published 20 May 2013)

We have measured the double-differential cross sections (DDCS) for electron emission in ionization of H_2O molecules under the impact of 4.5-MeV/u O^{8+} ions. The data were collected between 1 and 600 eV, in an angular range of 20°–150° by using an electrostatic hemispherical analyzer. In the experiment we used the H_2O vapor in a static gas condition which allowed us to deduce the absolute value of the cross sections. The single-differential cross sections (SDCS) and the total cross sections have also been obtained. The DDCS as well as the SDCS spectra are compared with the continuum-distorted-wave eikonal-initial-state (CDW-EIS) calculations for both the prior as well as the post forms of the scattering matrix. The initial state is represented within the complete neglect of differential overlap approximation, where the molecular orbitals are expressed in terms of atomic orbitals of the atomic constituents. The overall agreement with the CDW-EIS model is quite good as far as the energy dependence is concerned. The prior form of the model is found to provide a better understanding of the data compared to the post version. In particular, excellent agreement between the theory and experiment has been observed for the angular distribution data at forward angles.

DOI: 10.1103/PhysRevA.87.052710 PACS number(s): 34.50.Fa, 34.50.Gb

I. INTRODUCTION

Collisions of protons or highly charged ions (HCIs) with water molecules are of direct interest in radiation therapy [1,2]. The interaction of HCIs with biological tissues is responsible for generation of a large number of low-energy electrons. The role of these secondary electrons towards radiation damage is of great importance in cases of radiation therapy. In recent years there has been a substantial development in the field of hadron therapy using both protons as well as highly charged light ($Z \leqslant 10$) ions [2]. Precise measurements of the intensity and distribution of the emitted electrons are especially important in the region of the Bragg peak, since the largest part of the ion energy is deposited at that point. In fact, the ions have more favorable dose-depth distribution compared to photons, in terms of energy deposition near the Bragg peak region. Lately, studies involving ionization of large biomolecules from the biomedical therapy point of view, have become an important topic of research. For instance, the dependence of total ionization cross sections of uracil molecules on the projectile energy as well as charge state has been reported by Agnihotri *et al.* [3], using keV to MeV energy heavy ions. Similar studies with protons having different energies were reported earlier by many research groups [4–6].

It is well known that the total amount of water in a human body of average weight is 57% of the total body weight [7]. Hence, it is necessary to determine accurately the total as well as the differential cross sections for ionization of water molecules, in order to understand the inelastic processes induced by highly charged ions in biological matter. There have been numerous studies regarding the fragmentation of water molecules using projectiles such as protons [8–10], α particles [11], highly charged Ne ions [12], and C^{3+} and O^{5+} [13] ions. However, experimental measurements of differential and total cross sections for electron emission from water molecules are relatively scarce and the existing studies are limited to electrons [14], protons [15–20], and α particles [21–23], as projectiles. It is only in recent times, when measurements of absolute electron double-differential as well as single-differential cross sections for ionization of water molecules under the impact of bare carbon ions have been reported [24].

In addition to the importance of H_2O ionization studies towards biomedical therapy, it could serve as an important triatomic system to investigate fundamental ion molecule interaction processes. For instance, the two-center mechanism has been found to influence the angular distribution of the low-energy electron emission which has been studied in detail, mostly using targets such as H_2 [25–29] and He [30,31]. Double-differential cross section (DDCS) studies of low-energy electrons emitted in ionization of O_2 [32–34] and N_2 [35,36] under the impact of different projectiles have also been reported in a few recent investigations. However, such results are less reported for tri- or tetra-atomic molecules, except for a few theoretical [37] and experimental [38] studies involving CH_4 and CO_2 as targets.

In the present work, fast (velocity ∼13.43 a.u.), bare oxygen ions have been used to ionize the water molecules in vapor phase. The electron capture probability is quite low, as the σ_{capture} varies as $v_{\text{projectile}}^{-11}$ in the second-order Born approximation model [39]. Evidently, the dominant process for electron emission is the Coulomb ionization. We have investigated the details of the electron emission from H_2O, by measuring the absolute electron DDCS over a wide energy and angular range. Then, the data have been compared with both the prior as well the post version of the continuum-distorted-wave eikonal-initial-state (CDW-EIS) approximation. In this model, the initial bound state for multielectronic targets is described by means of a Hartree-Fock wave function,

*lokesh@tifr.res.in

distorted by a multiplicative eikonal phase representing the active electron in a continuum state of the projectile field. In the exit channel, the continuum of this active ionized electron is described by a double product of a plane wave and two continuum factors, each one of them associated with the residual target and the projectile fields. The passive electrons are, however, considered to remain as "frozen" in their initial orbitals. For calculating the transition matrix elements, an effective Coulomb potential is chosen to describe the interaction between the passive electrons and the active one in the final channel.

The paper has been divided into the following sections: an overview of the experimental assembly, details of the theoretical model, results and discussions, and conclusions.

II. EXPERIMENTAL ASSEMBLY

The present experiment was performed with 4.5-MeV/u O^{8+} ions available from the 14 MV Pelletron accelerator facility at TIFR, Mumbai. A poststripper assembly [40] along with the switching magnet was used to produce and select the required charge states of the ions. The beam was collimated into the desired size using a pair of four-jawed slits (2×2 mm^2) mounted one meter apart along the beam line, followed by another aperture of 4 mm diameter. A sufficient amount of deionized water was kept in a vacuum sealed container which in turn, was connected to the gas inlet of the interaction chamber via a solenoid valve. The base vacuum in the chamber was maintained at around 2×10^{-7} Torr. As the vapor pressure of water at room temperature (27 °C) is 27 Torr, water from the container entered the scattering chamber in vapor phase. The flow of water vapor inside the chamber was controlled by using a solenoid valve. A capacitance manometer (MKS Baratron) was used to measure the absolute pressure of the target gas inside the chamber. The whole chamber was flooded with water vapor at a pressure of 0.15 mTorr (i.e., ∼!0.02 Pa). The inner side of the scattering chamber was lined with two sets of thin μ-metal sheets (thickness 0.3 mm) in order to reduce the Earth's magnetic field at about 5–10 mG near the interaction region.

The secondary electrons emitted in the collision process were energy analyzed by a hemispherical, electrostatic spectrometer with its inner and outer electrodes having radii 2.5 and 3.5 cm, respectively. These energy analyzed electrons were finally detected using a channel electron multiplier (CEM) placed at the exit slit of the analyzer. For each emission angle, the electrons ejected with different energies were detected for a specified amount of incident projectile charge collected on a Faraday cup.

The absolute double-differential cross sections were measured at a given emission angle, by using the electron spectrum obtained with and without the target gas. The following relation [41] was used:

$$\frac{d^2\sigma}{d\Omega_e d\epsilon_e} = \frac{\frac{N_e(\epsilon_e,\theta e)}{N_p \Delta\epsilon} - \frac{N_b(\epsilon_e,\theta e)}{N'_p \Delta\epsilon}}{n(l\Omega)_{\rm eff}\eta_{\rm el}}. \tag{1}$$

Here, $n = 9.659 \times 10^{15} P_c$ (mTorr)/T (K) is the number density of the target gas molecules in units of cm^{-3}, under a static gas pressure condition. The quantities N_e and N_b are the number of electrons detected in the presence and absence of the target gas, respectively. The number of incident projectile ions is represented as N_p and N'_p, in the presence and absence of the target gas, respectively. The quantity $\Delta\epsilon$ is the energy resolution of the spectrometer, which is typically 6% of the electron energy. The detection efficiency of the CEM, $\eta_{\rm el}$, is taken to be 0.9 as mentioned in the operation manual [42] of the CEM used. For this purpose, the "front" of the CEM was kept at +100 V. Finally, the $(l\Omega)_{\rm eff}$ is the solid-angle path-length integral given by $\frac{w_1 w_2 h_2}{LR\sin\theta}$. Here, w_1 is the width for the entrance slit, and w_2 and h_2 are, respectively, the width and height of the exit slit of the spectrometer [41]. The length of the collimator is given by L and R is the distance of the collimator from the center of the interaction zone.

The energy dependence of the electron DDCS was studied for 11 different angles: 20°, 30°, 45°, 60°, 75°, 80°, 90°, 105°, 120°, 135°, and 150°. At each angle the emitted electrons having energies between 1 and 600 eV were detected. Some of the representative values of the absolute electron DDCS have been tabulated in Table I. The counts due to background (N_b) were low (∼10% of the total counts) in the low-energy regions (<100 eV). In general, the error due to statistical fluctuation was 8%–15%, for most of the emission angles. However, for the extreme backward angles (e.g., 135° and 150°), it was larger (∼20%) in the higher emission energies (> 500 eV), due to an increase in the background counts. The uncertainty in the gas pressure was about 6%–7%. Overall, the maximum absolute error in the data presented here is about 15%–25%.

III. THEORETICAL MODELS

The theoretical model used in this work to describe the electron emission process is the continuum-distorted-wave eikonal-initial-state (CDW-EIS) one [43,44]. In the distorted-wave formalism, the action of the perturbative potentials can either be applied to the initial channel distorted–wave function or to the final channel distorted one, giving rise to the *prior* and *post* versions of the transition matrix element, respectively. In the first-order approximation of its prior version as a function of the impact parameter ($\vec{\rho}$), we have

$$\mathcal{A}^-_{if}(\vec{\rho}) = -i\int_{-\infty}^{+\infty} dt\, \langle \chi^-_f | (W_i | \chi^+_i \rangle). \tag{2}$$

In Eq. (2) χ^+_i and χ^-_f are the initial and final channel distorted-wave functions, and W_i is the well-known EIS perturbative operator ([45,46]).

For the post version, in the exit channel, the target potential is usually approximated by an effective Coulombic one $V_T(\vec{x}) \simeq -Z_T^{\rm eff}/x$, where $\vec{x}$ is the position of the active electron in a target-fixed reference frame, $Z_T^{\rm eff}$ is an effective target charge chosen to preserve the binding energy ε_i of the active electron initial orbital, i.e., $Z_T^{\rm eff} = n_i\sqrt{-2\varepsilon_i}$, with n_i the principal quantum number of the orbital. Thus, the post version of the scattering amplitude reads

$$\mathcal{A}^+_{if}(\vec{\rho}) = -i\int_{-\infty}^{+\infty} dt\, (\langle \chi^-_f | W^\dagger_f) | \chi^+_i \rangle. \tag{3}$$

In Eq. (3) W_f is the widely used CDW perturbative operator ([45,46]).

TABLE I. Measured double-differential cross sections in units of Mb eV^{-1} sr^{-1} for different emission angles. Typical errors are 15%–20% (see text) except for, high-energy (>200 eV) electrons emitted at large backward angles (135° and 150°), for which the uncertainties could be about 25%.

Energy (ev)	20°	30°	45°	60°	75°	80°	90°	105°	120°	135°	150°
3	3.2246	5.4486	12.4197	15.5183	16.3977	12.8585	12.1168	11.8072	6.7081	7.3097	6.5644
5	3.3869	4.5501	12.4437	11.9763	10.6546	9.7742	8.9809	8.5861	5.3708	5.3962	4.5223
11	2.2029	2.7416	5.3311	5.1809	5.4141	4.0367	4.5865	4.0869	2.6710	2.5108	2.0015
15	1.7359	1.8917	3.5381	3.6478	3.8859	3.0330	3.4580	3.0906	1.9020	1.6022	1.3051
20	1.2463	1.3989	2.4279	2.5018	2.8106	2.6544	2.4116	1.8303	1.1846	1.0099	0.8242
40	0.4490	0.4799	0.7756	0.9831	1.2017	1.0984	0.8778	0.6996	0.3571	0.2389	0.1628
60	0.1852	0.2207	0.3591	0.4580	0.6715	0.7001	0.4758	0.2765	0.1484	0.0907	0.0535
80	0.1127	0.1160	0.1905	0.2211	0.4244	0.4361	0.3080	0.1581	0.0980	0.0440	0.0315
100	0.0723	0.0741	0.1371	0.1489	0.3086	0.3159	0.2304	0.0898	0.0446	0.0187	0.0184
140	0.0341	0.0327	0.0566	0.0746	0.2377	0.1989	0.1298	0.0418	0.2043	0.0064	0.0080
180	0.0209	0.0217	0.0396	0.3962	0.1569	0.1458	0.0890	0.0215	0.0079	0.0033	0.0054
200	0.0163	0.0152	0.0319	0.0346	0.1133	0.0909	0.0526	0.0218	0.0065	0.0029	0.0039
240	0.0102	0.0106	0.0196	0.0302	0.0809	0.0789	0.0464	0.0138	0.0054	0.0020	0.0028
280	0.0051	0.0071	0.0160	0.0220	0.0564	0.0601	0.0269	0.0098	0.0044	0.0018	0.0019
320	0.0043	0.0054	0.0139	0.0158	0.0421	0.0504	0.0219	0.0081	0.0042	0.0016	0.0018
360	0.0033	0.0041	0.0120	0.0127	0.0352	0.0287	0.0189	0.0067	0.0037	0.0014	0.0015
400	0.0043	0.0036	0.0117	0.0099	0.0342	0.0215	0.0184	0.0075	0.0038	0.0028	0.0015
460	0.0115	0.0101	0.0152	0.0252	0.0410	0.0274	0.0202	0.0153	0.0112	0.0107	0.0103
500	0.0062	0.0091	0.0097	0.0142	0.0326	0.0194	0.0372	0.0109	0.0059	0.0052	0.0068
560	0.0014	0.0027	0.0051	0.0079	0.0297	0.0113	0.0146	0.0069	0.0026	0.0017	0.0012
600	0.0012	0.0023	0.0030	0.0061	0.0291	0.0085	0.0149	0.0047	0.0015	0.0011	0.0005

Approximating V_T by an effective Coulomb potential leads to the partial omission of a potential related to the dynamic screening produced by the passive electrons on the evolution of the active one in the exit channel. Therefore the results arising from the post version of the CDW-EIS model will differ from those obtained using the prior one. Recently Monti *et al*. [46,47] have shown that the inclusion of this residual potential in the post version of the CDW-EIS model almost completely diminishes these post-prior discrepancies. Finally, the doubly differential cross section as a function of the emitted electron energy (E_k) and solid angle (Ω_k) is defined as

$$\frac{d^2\sigma}{dE_k d\Omega_k} = k \int d\vec{\rho}\, |\mathcal{A}_{if}^{\pm}(\vec{\rho})|^2. \tag{4}$$

IV. RESULTS AND DISCUSSIONS

A. DDCS: Energy distributions

The measured energy distributions of absolute DDCS for electron emission at six different emission angles have been shown in Fig. 1. The cross section reaches a large value in the low (< 15 eV) energy region due to the dominance of the soft collision process involving a large impact parameter. The cross section then decreases over several orders of magnitude with the increase in the emission energy. The peak at around 480 eV corresponds to the oxygen K-LL Auger electron emission. The total Auger cross section, as obtained from the experimental data, is ∼11 Mb. This value has been compared with the prediction of the ECPSSR (perturbed stationary state model with energy loss Coulomb deflection and relativistic corrections) model [48], which is commonly used for the inner-shell ionization processes. The corresponding value, using the ECPSSR model, is approximately 14 Mb for the collision system 4.5-MeV/u O^{8+} + O. The experimental value is thus well within the range of validity of this model, which

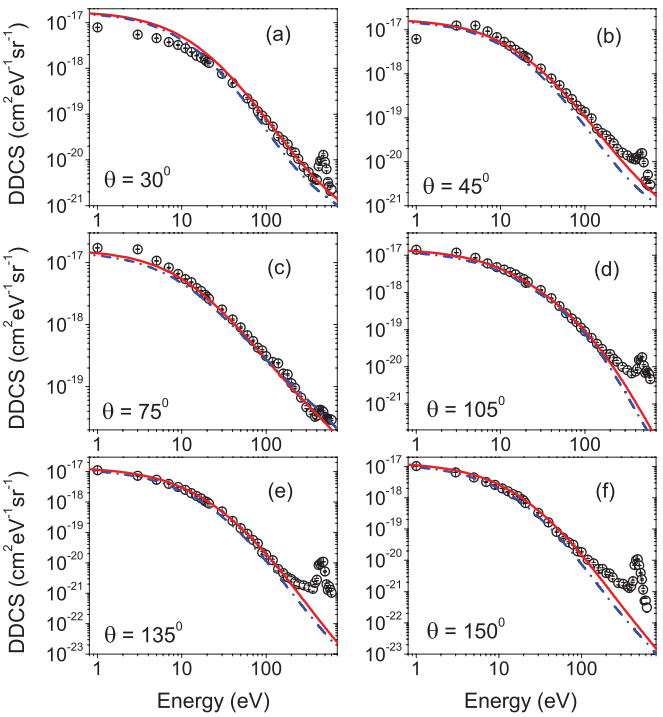

FIG. 1. (Color online) The absolute electron DDCS for different emission angles. In each plot, the solid (dash-dotted) red (blue) line corresponds to the CDW-EIS prior (post) version.

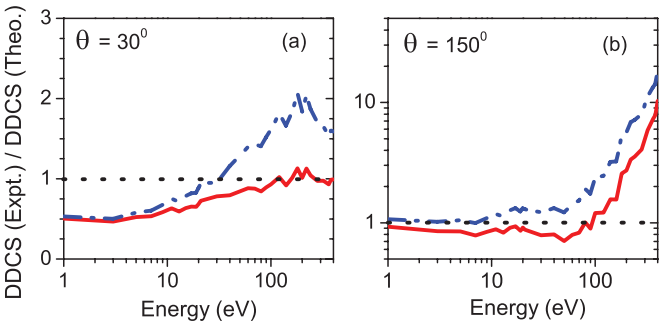

FIG. 2. (Color online) Ratio of the experimental DDCS to the theoretical one, for 30° and 150°. The solid (dash-dotted) red (blue) line corresponds to the ratio for the CDW-EIS prior (post) version. The dotted horizontal line denotes the ratio = 1.

typically reproduces the data within an approximate factor of 2, based on the target-projectile combination. This serves as a reasonable cross-check on the measured data.

The experimental data have been compared with the theoretical calculations using the CDW-EIS model. Both the prior as well as the post version of the model have been used. Overall, a qualitative agreement between both the theoretical approximations and the data can be seen for different emission angles. However, a closer inspection shows substantial deviation of the experimental data from theoretical values at energies >200 eV, especially for the extreme backward angles [see Figs. 1(e) and 1(f)]. A good quantitative agreement could be seen for energies 5–150 eV, for all angles. An excellent agreement with the data at 75°, throughout the entire energy range, may be noted. A good agreement between 1 and 200 eV, for 105° and 135°, can also be seen.

For better presentation, the obtained data have been divided by the corresponding theoretical values (both prior and post versions) at each emission energy (see Fig. 2). At 30°, in the case of the prior version [solid line in Fig. 2(a)], the ratio starts from 0.5 at very low energies (∼1 eV) and reaches the value 1 at around 150 eV. At energies >150 eV, the ratio remains close to 1, implying a good agreement between the data and the prior version. However, for the post version [dashed-dotted line in Fig. 2(a)], the ratio starts from 0.5, reaches 1 at around 30 eV and increases further up to 2, at around 200 eV. After that, it gradually decreases and finally, reaches the value 1.5 at 400 eV. Evidently, in this case, the post version underestimates the data from 30 to 400 eV.

Similarly, at 150°, the ratio (for the prior version) is close to unity, mostly in the low-energy (1–100 eV) region [solid line in Fig. 2(b)], beyond which the theory underestimates the data. However, the post version [dashed-dotted line in Fig. 2(b)] matches quantitatively well with the data, only up to 50 eV. It underestimates the data at all energies from 50 to 400 eV.

It should be noted that the quantitative agreement between the data and the CDW-EIS prior version is better compared to that between the data and the post version. It can be explained in terms of the fact that the post version does not consider the inclusion of perturbative potentials which take into account the short range part of the electron dynamic screening. As a result the post version underestimates the results obtained with the prior approximation [46].

Also, it must be mentioned that the theoretical model does not take into account any inner-shell ionization process and some deviations could be seen in the higher-energy region 400–600 eV [see Figs. 1(a)–1(f)]. At 75° [see Fig. 1(c)], the Auger emission peak is not observed to be well pronounced, which may be due to the dominance of the binary counter process, at that particular angle.

B. DDCS: Angular distributions

Figure 3 shows the angular distributions of the absolute electron DDCS at different energies of the emitted electrons. Overall, the theoretical models (both prior and post) have qualitatively reproduced the shape of the experimental data. As far as the absolute values are concerned, very good quantitative agreement with the prior version can be seen for energies 20, 40, 100, and 200 eV [see Figs. 3(a)–3(d)]. However, substantial deviation from the experiment can be seen at high emission energies (240 and 320 eV) and at extreme backward angles [see Figs. 3(e) and 3(f)].

At relatively low energy such as at 20 eV, the DDCS values at extreme forward angles and those at extreme backward angles are relatively close to each other, e.g., σ_{DDCS} is ∼1.2 Mb eV^{-1} sr^{-1} at 20° and ∼0.8 Mb eV^{-1} sr^{-1} at 150° [see Fig. 3(a)]. But as the emission energy increases this relative difference between forward and backward DDCS increases more and more. For example at 100 eV σ_{DDCS} is ∼0.07 Mb eV^{-1} sr^{-1} at 20° and ∼0.02 Mb eV^{-1} sr^{-1} at

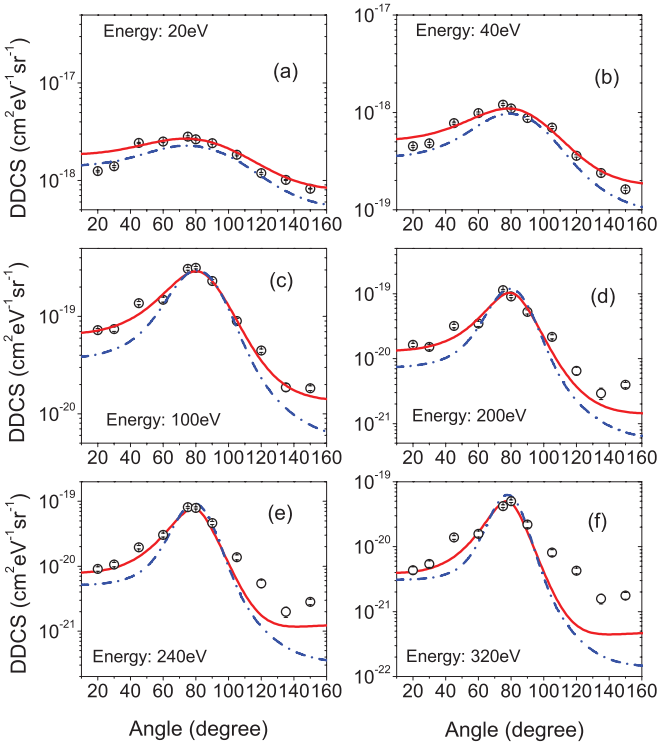

FIG. 3. (Color online) Angular distributions of the absolute electron DDCS at fixed emission energies. In each plot, the solid (dash-dotted) red (blue) line corresponds to the CDW-EIS prior (post) version.

150° [see Fig. 3(c)]. This large forward-backward angular asymmetry was already observed earlier for different atomic (e.g., H, He, Ne, etc.) as well as molecular (e.g., H_2, N_2, O_2, etc.) targets and can be explained in terms of the two-center effect (TCE). As the ejected electron gets more and more influenced by the two Coulombic centers, namely, the receding projectile ion and the residual recoil ion, it can undergo a significant amount of successive or simultaneous deflection in this two-center field. Consequently, the cross sections in the forward angles get enhanced due to the strong attraction of the emitted electrons by the receding projectile ions moving in the same direction. Evidently, extremely low-energy electrons (<10 eV) are least affected by TCE, because their velocities are very small compared to that of the projectile ions. In the present case, the prior version has approximately reproduced the angular asymmetry in the experimental data, whereas the post version has predicted a much higher asymmetry in all the cases.

In addition, the angular distributions gradually become more peaked around 75°–80°, as one increases the emission energy. The difference in the shape of the distributions for low- and high-energy electrons is due to the binary nature of collision [49]. For collision between a fast projectile ion and an electron initially at rest, corresponding to a given amount of energy transfer, the electron goes off in a well-defined direction giving a Dirac δ-function angular distribution. However, if the target electron is initially bound, the binding energy decides its initial momentum distribution in the target atom. This momentum distribution causes a change in the relative velocity of the incident ion and the target electron. Consequently, the probability of ejection of the electrons broadens over an angular range, which smears out the previous Dirac δ-function distributions. It has been shown elsewhere [50], that the position of the Dirac δ function, under binary encounter approximation, is given by $\cos^2\theta = \frac{E}{2m_e V_p^2}$. Here, E is the energy of the ejected electron with mass m_e and V_p is the velocity of the projectile ion. In the present case, this semiclassical approximation matches quite well with the experimental data. For example, in the case of an emitted electron with energy 100 eV, the previous formula predicts the position of the binary peak to be at 82°, whereas the experimental value is approximately 80° [see Fig. 3(c)]. Similarly, the position of the peak is at 81°, under the CDW-EIS (both post and prior versions) approximation. However, the three-body mechanism (including the TCE) also influences the angular distributions and hence, the peak position cannot be fully explained by the binary encounter model alone.

C. Single-differential and total cross sections

The single-differential cross sections (SDCS) in emission angles can be obtained by integrating the DDCS over the ejected electron energy ϵ_e as

$$\frac{d\sigma}{d\Omega_e} = \int_{\epsilon_i}^{\epsilon_f} \frac{d^2\sigma}{d\Omega_e d\epsilon_e} d\epsilon_e. \tag{5}$$

Figure 4 shows the angular distribution of SDCS ($\frac{d\sigma}{d\Omega}$), for the emitted electrons. The experimental DDCS values have been integrated over an energy range of 1–400 eV (excluding the Auger region), for obtaining the SDCS values. The distribution has been quantitatively well reproduced by the theoretical model, though relatively large deviations can be seen in the extreme forward angles. This can be attributed to the fact that a significant contribution to the SDCS comes from the DDCS of the low-energy (1–20 eV) electrons. For 20° and 30°, both the theoretical models overestimate the experimental DDCS by an approximate factor of 1.8–2.0, in the energy region 1–20 eV.

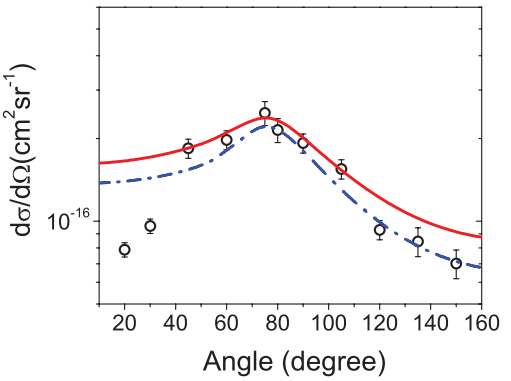

FIG. 4. (Color online) The absolute electron SDCS at different emission angles. The solid (dash-dotted) red (blue) line corresponds to the CDW-EIS prior (post) version.

Similarly, the SDCS in emission energies can be obtained by integrating the DDCS over the solid angle Ω_e of emission as

$$\frac{d\sigma}{d\epsilon_e} = \int_{\Omega_i}^{\Omega_f} \frac{d^2\sigma}{d\Omega_e d\epsilon_e} d\Omega_e = 2\pi \int_{\theta_i}^{\theta_f} \frac{d^2\sigma}{d\Omega_e d\epsilon_e} \sin\theta \, d\theta_e. \tag{6}$$

Figure 5 shows the energy distribution for the electron SDCS ($\frac{d\sigma}{d\epsilon}$). The experimental DDCS values have been integrated over an angular range of 20°–150°, for obtaining the SDCS values. For angles less than 20° and more than 150°, the contribution was small and was estimated by extrapolating. The distribution has been quantitatively well reproduced by both the theoretical models, over the entire energy range 1–400 eV.

The total cross section obtained from the experimental data (interpolated from 0° to 180°) is ∼2.0 Gb. Similarly, the total cross section obtained from the CDW-EIS prior version is

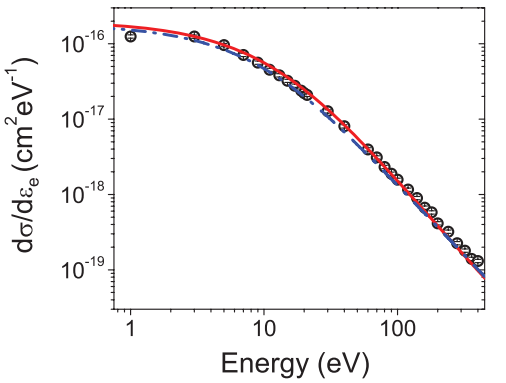

FIG. 5. (Color online) The absolute electron SDCS at different emission energies. The solid (dash-dotted) red (blue) line corresponds to the CDW-EIS prior (post) version.

2.1 Gb and that obtained from the post version is 1.8 Gb. Evidently, the experimental value is within 5% of that obtained from the prior version, whereas the post version underestimates the experimental value by an approximate factor of 1.1.

V. CONCLUSION

In conclusion, we have reported the absolute doubly differential cross section as a function of ejection energy and angle, for electron emission from water molecules. A stringent test has been provided to the post and prior versions of the CDW-EIS model. The DDCS values obtained from the experiment have better quantitative agreement with the prior version as compared to the post version. In general, an excellent match between the prior model and experiment could be found for most of the angles and for energies 1–200 eV, except at extreme backward angles. However, substantial deviation between the data and both the theoretical models, has been observed at energies above 200 eV, over different emission angles. The single-differential cross sections obtained by integrating the experimental DDCS are also in quantitative agreement with the theoretical calculations. The absolute value of the total cross section was found to be 2.0 Gb, which matches quite well with the prediction of the theoretical calculations.

ACKNOWLEDGMENT

We would like to thank the staff at BARC-TIFR Pelletron accelerator facility for smooth operation of the machine.

[1] R. R. Wilson, Radiology **47**, 487 (1946).
[2] U. Amaldi and G. Kraft, Rep. Prog. Phys. **68**, 1861 (2005).
[3] A. N. Agnihotri, S. Kasthurirangan, S. Nandi, A. Kumar, M. E. Galassi, R. D. Rivarola, O. Fojón, C. Champion, J. Hanssen, H. Lekadir, P. F. Weck, and L. C. Tribedi, Phys. Rev. A **85**, 032711 (2012).
[4] P. Moretto-Capelle and A. Le Padellec, Phys. Rev. A **74**, 062705 (2006).
[5] J. Tabet, S. Eden, S. Feil, H. Abdoul-Carime, B. Farizon, M. Farizon, S. Ouaskit, and T. D. Märk, Phys. Rev. A **82**, 022703 (2010).
[6] Y. Iriki, Y. Kikuchi, M. Imai, and A. Itoh, Phys. Rev. A **84**, 032704 (2011).
[7] A. C. Guyton, *Textbook of Medical Physiology*, 5th ed. (W. B. Saunders, Philadelphia, 1976), p. 424.
[8] U. Werner, K. Beckord, J. Becker, and H. O. Lutz, Phys. Rev. Lett. **74**, 1962 (1995).
[9] F. Alvarado, R. Hoekstra, and T. Schlathölter, J. Phys. B **38**, 4085 (2005).
[10] M. Murakami, Tom Kirchner, M. Horbatsch, and H. J. Lüdde, Phys. Rev. A **85**, 052713 (2012).
[11] P. Sobocinski, Z. D. Pešić, R. Hellhammer, N. Stolterfoht, B. Sulik, S. Legendre, and J.-Y. Chesnel, J. Phys. B **38**, 2495 (2005).
[12] Z. D. Pešić, J-Y. Chesnel, R. Hellhammer, B. Sulik, and N. Stolterfoht, J. Phys. B **37**, 1405 (2004).
[13] H. Luna and E. C. Montenegro, Phys. Rev. Lett. **94**, 043201 (2005).
[14] M. A. Bolorizadeh and M. E. Rudd, Phys. Rev. A **33**, 882 (1986).
[15] L. H. Toburen and W. E. Wilson, J. Chem. Phys. **66**, 5202 (1977).
[16] M. E. Rudd, T. V. Goffe, R. D. DuBois, and L. H. Toburen, Phys. Rev. A **31**, 492 (1985).
[17] M. A. Bolorizadeh and M. E. Rudd, Phys. Rev. A **33**, 888 (1986).
[18] O. Boudrioua, C. Champion, C. Dal Cappello, and Y. V. Popov, Phys. Rev. A **75**, 022720 (2007).
[19] L. F. Errea, Clara Illescas, L. Méndez, B. Pons, I. Rabadán, and A. Riera, Phys. Rev. A **76**, 040701(R) (2007).
[20] H. J. Lüdde, T. Spranger, M. Horbatsch, and T. Kirchner, Phys. Rev. A **80**, 060702(R) (2009).
[21] L. H. Toburen, W. E. Wilson, and R. J. Popowich, Radiat. Res. **82**, 27 (1980).
[22] D. Ohsawa, Y. Sato, Y. Okada, V. P. Shevelko, and F. Soga, Phys. Rev. A **72**, 062710 (2005).
[23] C. Champion, O. Boudrioua, C. Dal Cappello, Y. Sato, and D. Ohsawa, Phys. Rev. A **75**, 032724 (2007).
[24] C. Dal Capello, C. Champion, O. Boudrioua, H. Lekadir, Y. Sato, and D. Ohsawa, Nucl. Instrum. Methods Phys. Res., Sect. B **267**, 781 (2009).
[25] Lokesh C. Tribedi, P. Richard, Y. D. Wang, C. D. Lin, and R. E. Olson, Phys. Rev. Lett. **77**, 3767 (1996).
[26] N. Stolterfoht, B. Sulik, V. Hoffmann, B. Skogvall, J.-Y. Chesnel, J. Rangama, F. Frémont, D. Hennecart, A. Cassimi, X. Husson, A. L. Landers, J. A. Tanis, M. E. Galassi, and R. D. Rivarola, Phys. Rev. Lett. **87**, 023201 (2001).
[27] D. Misra, U. Kadhane, Y. P. Singh, L. C. Tribedi, P. D. Fainstein, and P. Richard, Phys. Rev. Lett. **92**, 153201 (2004).
[28] F. Frémont, A. Hajaji, A. Naja, C. Leclercq, J. Soret, J. A. Tanis, B. Sulik, and J.-Y. Chesnel, Phys. Rev. A **72**, 050704(R) (2005).
[29] D. Misra, A. Kelkar, U. Kadhane, A. Kumar, L. C. Tribedi, and P. D. Fainstein, Phys. Rev. A **74**, 060701(R) (2006).
[30] N. Stolterfoht, H. Platten, G. Schiwietz, D. Schneider, L. Gulyas, P. D. Fainstein, and A. Salin, Phys. Rev. A **52**, 3796 (1995).
[31] D. Misra, A. H. Kelkar, P. D. Fainstein, and L. C. Tribedi, J. Phys. B: At. Mol. Opt. Phys. **45**, 225201 (2012).
[32] M. Winkworth, P. D. Fainstein, M. E. Galassi, J. L. Baran, B. S. Dassanayake, S. Das, A. Kayani, and J. A. Tanis, Nucl. Instrum. Methods Phys. Res., Sect. B **267**, 373 (2009).
[33] S. Nandi, A. N. Agnihotri, S. Kasthurirangan, A. Kumar, C. A. Tachino, R. D. Rivarola, F. Martín, and L. C. Tribedi, Phys. Rev. A **85**, 062705 (2012).
[34] S. Nandi, A. N. Agnihotri, C. A. Tachino, R. D. Rivarola, F. Martín, and L. C. Tribedi, J. Phys. B **45**, 215207 (2012).
[35] J. L. Baran, S. Das, F. Járai-Szábo, K. Póra, L. Nagy, and J. A. Tanis, Phys. Rev. A **78**, 012710 (2008).
[36] C. A. Tachino, F. Martín, and R. D. Rivarola, J. Phys. B **45**, 025201 (2012).
[37] M. E. Galassi, R. D. Rivarola, M. Beuve, G. H. Olivera, and P. D. Fainstein, Phys. Rev. A **62**, 022701 (2000).
[38] C. Dimopoulou, M. E. Galassi, R. Moshammer, R. D. Rivarola, D. Fischer, C. Höhr, and J. Ullrich, J. Phys. B **38**, 3173 (2005).

[39] M. R. C. Mcdowell and J. P. Coleman, *Introduction to the Theory of Ion-Atom Collisions* (North Holland, Amsterdam, 1970), Chap. 8.
[40] S. D. Narvekar, R. R. Hosangdi, L. C. Tribedi, R. G. Pillay, K. G. Prasad, and P. N. Tandon, Pramana **39**, 79 (1992).
[41] D. Misra, K. V. Thulasiram, W. Fernandes, A. H. Kelkar, U. Kadhane, A. Kumar, Y. P. Singh, L. Gulyas, and L. C. Tribedi, Nucl. Instrum. Methods Phys. Res., Sect. B **267**, 157 (2009).
[42] Channel Electron Multiplier, Dr. Sjuts Optotechnik GmbH, Germany (2002).
[43] D. S. F. Crothers and J. F. McCann, J. Phys. B **16**, 3229 (1983).
[44] P. D. Fainstein, V. H. Ponce, and R. D. Rivarola, J. Phys. B **21**, 287 (1988).
[45] P. D. Fainstein, V. H. Ponce, and R. D. Rivarola, J. Phys. B **24**, 3091 (1991).
[46] J. M. Monti, O. A. Fojón, J. Hanssen, and R. D. Rivarola, J. Phys. B **43**, 205203 (2010).
[47] J. M. Monti, O. A. Fojón, J. Hanssen, and R. D. Rivarola, J. At. Mol. Opt. Phys. **2010**, 128473 (2010).
[48] W. Brandt and G. Lapicki, Phys. Rev. A **23**, 1717 (1981).
[49] S. T. Manson, L. H. Toburen, and N. Stolterfoht, Phys. Rev. A **12**, 60 (1975).
[50] T. F. M. Bonsen and L. Vriens, Physica **47**, 307 (1970).